Title:

Clinical characteristics and high resolution retinal imaging of retinitis pigmentosa caused by *RP1* gene variants

Running title: Clinical and AO findings in RP1-ARRP

Authors: Shinji Ueno[1], Yoshito Koyanagi [1,2], Taro Kominami [1], Yasuki Ito [1], Kawano Kenichi [1], Koji M Nishiguchi [3], Carlo Rivolta [4,5,6], Toru Nakazawa[3], Koh-Hei Sonoda [2] and Hiroko Terasaki[1]

Institutions:

[1] Department of Ophthalmology, Nagoya University Graduate School of Medicine, Nagoya, Japan
[2] Department of Ophthalmology, Graduate School of Medical Sciences, Kyushu University, Fukuoka, Japan
[3] Department of Ophthalmology, Tohoku University Graduate School of Medicine, Sendai, Japan
[4] Institute of Molecular and Clinical Ophthalmology Basel (IOB), Basel, Switzerland
[5] University of Basel, Basel, Switzerland
[6] Department of Genetics and Genome Biology, University of Leicester, Leicester, UK

***Correspondence:** Shinji Ueno, M.D., Ph.D., Department of Ophthalmology, Nagoya University Graduate School of Medicine, 65 Tsuruma-cho, Showa-ku, Nagoya 466-8550, Japan
Tel: +81-52-744-2277, Fax: +81-52-744-2278

E-mail: ueno@med.nagoya-u.ac.jp

Word count; (abstract) 241 (main text) 3316
Total number of references; 26
Total number of figures; 8 figures
Total number of table; 1

Abstract

Purpose: To report the clinical course and high resolution images with autosomal recessive retinitis pigmentosa (RP) associated with a variant of the *RP1* gene (c.4052_4053ins328/p.Tyr1352Alafs*9; m1). This variant has been found to be a high frequency founder variant in Japanese RP patients.

Study Design: Retrospective case series

Methods: Nine patients from 5 unrelated Japanese families were studied. Five patients had the m1 variant homozygously, and 4 patients had the m1 variant compound heterozygously with another frameshift variant, (c.4196delG/p.Cys1399Leufs*5). Ophthalmic examinations including adaptive optics (AO) fundus imaging were performed periodically.

Results: The fundus photographs, fundus autofluorescence (FAF) images, and optical coherence tomographic (OCT) images indicated severe retinal degeneration involving the macula even at a young age (20s) in all the patients. The areas of surviving photoreceptor in the central macula were seen as hyper-autofluorescent regions in the FAF images and preserved outer retinal structure in the OCT images, and they were identifiable in the AO fundus images in 8 eyes. The borders of the surviving photoreceptor areas were surrounded by hyporeflective clumps, presumably containing melanin, and the size of these areas decreased progressively during the 4-year follow-up period. The disappearance of the surviving photoreceptor areas was associated with complete blindness.

Conclusion: Patients with RP associated with the m1 variant have a progressive and severe retinal

45 degeneration that begins at an early age. Monitoring the surviving photoreceptor areas by AO fundus

46 imaging can provide a more precise pathological progress of the retinal degeneration.

47

Keywords: Autosomal recessive retinitis pigmentosa; *RP1*; Adaptive optics images; Fundus autofluorescence

Introduction

Retinitis pigmentosa (RP) represents a heterogeneous group of retinal disorders that is characterized by a progressive degeneration of both the rod and cone photoreceptors bilaterally. The *RP1* gene was the first gene identified to cause autosomal dominant RP (adRP) [1, 2], and it was later found to also cause autosomal recessive RP (arRP) [3-6]. Recently, *RP1* was reported to be associated with autosomal recessive macular dystrophy and autosomal recessive cone-rod dystrophy [7, 8]. *RP1* encodes a multimodular protein of 2156 amino acids, and it is a member of the doublecortin family. *RP1* is present in the ciliary axoneme of both rods and cones [9]. Mutations in *RP1* is associated with a decrease in the best-corrected visual acuity (BCVA) which is due to a ciliopathic phenotype caused by an abnormal stacking of the outer segment discs of rods and cones [10].

To date, at least 170 mutations have been reported in *RP1,* and most of these mutations cluster within its last exon, exon 4, cumulatively accounting for approximately for 5.5% of all adRP and up to 4.5% of all autosomal arRP cases [5, 11].

Our earlier study by whole-genome sequence screening of Japanese patients identified a new, unusual mutation consisting of an insertion of a mobile *Alu* element in exon 4 of the *RP1* gene (c.4052_4053ins328/p.Tyr1352Alafs*9 ; m1) [12]. This m1 insertion variant causes a disruption of the reading frame by introducing 328 additional nucleotides and a premature termination codon in the canonical *RP1* coding sequence. Additional targeted screening for the m1 variant in 330

71 Japanese patients identified 15 other Japanese individuals who carried this variant [12]. These
72 findings indicated that m1 is a relatively frequent cause of retinal degeneration in the Japanese RP
73 patients. However, precise phenotypic analyses were not performed in these earlier studies. Thus,
74 the purpose of this study was to determine the pattern of progression of the retinal degeneration in
75 arRP patients with the m1 variant of the *RP1* gene using adaptive optics (AO) fundus imaging.
76
77 **Methods**
78 This was an observational case series conducted at Nagoya University Hospital. The study protocol
79 adhered to the tenets of the Declaration of Helsinki and was approved by the Institutional Review
80 Board of Nagoya University (approval number: 2010-1067). A written informed consent was
81 obtained from all participants. We studied 9 patients from 5 unrelated families in whom the m1
82 mutation had been identified.
83
84 **Genetic analyses.** In all families, genomic DNA was extracted from peripheral lymphocytes
85 according to standard procedures. The genetic data of patients NA0039, NA1039, NA0070, NA0201,
86 NA1201, and NA0209 were obtained earlier by whole genome sequencing and direct sequencing
87 [12].The m1 and another frameshift variant (c.4196delG/p.Cys1399Leufs*5, m2) in patients
88 NA1048 and NA1201 and some of the unaffected family members were analyzed in this study. A

89 pair of primers was designed to screen for the presence of the m1 and m2 variants in exon 4 of the
90 *RP1* gene;forward: 5′- AGGCTTGTTTCCTAGGAGAGGT-3′, reverse: 5′-
91 TTCTGCTTCTTTTTCACTTAGGC-3′. The presence of m1 variant was confirmed from the
92 differences in the size of the polymerase chain reaction (PCR) product by electrophoresis. The PCR
93 products were purified and both strands of the gene were sequenced with an automated sequencer
94 (Fasmaq, Atsugi, Kanagawa, Japan).
95
96 **Clinical Evaluations.** Clinical data were obtained from the medical records. All patients had visual
97 acuity measurements, Goldmann perimetry, conventional fundus photographs, and spectral-domain
98 optical coherence tomography (SD-OCT, Spectralis; Heidelberg Engineering, Heidelberg, Germany).
99 Fundus autofluorescence (FAF) imaging was performed with an ultra-widefield imaging device
100 (Optos P200Tx; Optos, Dunfermline, UK) in 8 patients.
101 Fundus images with microscopic resolution were obtained using the flood-illuminated AO retinal
102 camera (rtx1, Imagine Eyes, Orsay, France). This system was used in an earlier investigations to
103 obtain images of individual cone photoreceptors [13-16]. Montage images were constructed within
104 6° of the fovea using the i2k Retina software (DualAlign LLC, Clifton Park, NY, USA). The
105 densities of the cone photoreceptors in NA0209 and one normal control eye were automatically
106 calculated using a software (AO detect v0.1, Imagine Eyes, France) and subsequently corrected

manually as described[13, 15, 16]. The area of analysis was 80 × 80 pixels or approximately 65 μm x 65 μm at 1° and 3° from the fovea on the nasal side and 3° from the fovea on the temporal side. To measure the size of surviving photoreceptor area, the processed images were analyzed with the ImageJ software (version 1.48; the National Institutes of Health, Bethesda, MD, USA). The axial length (AL) was obtained by the IOL Master (Carl Zeiss Meditec, Dublin, CA), and the AL was used to adjust for the different degrees of magnification caused by differences in the AL.

The decimal BCVA was converted to the logarithm of the minimum angle of resolution (logMAR) units for the statistical analyses. Counting fingers (CF), hand motion (HM), light perception (LP), and no light perception, were designated as 1.85, 2.30, 2.80, and 2.90 logMAR units, respectively.

Results

Nine affected patients from 5 families with a clinical diagnosis of RP and harboring m1 variants were studied. Five patients from 3 families had the m1 variant homozygously and 4 patients from 2 families had the m1 variant compound heterozygously with another frameshift variant (c.4196delG/p.Cys1399Leufs*5, m2). The pedigrees of the 5 families are presented in Figure 1. All five families were originally from Japan, and any mixture with other ethnicities was not reported. Autosomal recessive family history was reported in 4 families and sporadic case was reported in one

family (Family #3). The parents of the patients were not affected even though they have the m1 or m2 variant heterozygously.

The demographics of the clinical characteristics are presented in Table. The mean age was 17.9 ± 6.2 years with a range of 8 to 27 years at the initial examination and that was 30.4 ± 6.5 years with a range of 19 to 39 years at the last examination. The mean and median observation period was 12.2 years and 13 years respectively. The initial symptom of all patients was night blindness and 8 patients experienced it from their childhood, while one patient (NA0209) first noted the night blindness at age 15 years.

Visual acuity.

Even at the initial visit, the BCVA was worse than 1.0 (decimal visual acuity) in 8 of the patients. BCVA was worse than 0.3 in the better eye in 5 patients at the last examination. The visual fields were severely constricted even at a young age, and most of the patients had paracentral scotomata with peripheral constriction or a central island. Electroretinograms (ERGs) were barely recordable in 2 patients and non-recordable in the remaining 6 patients (ERG data of NA1039 was unavailable.). These findings indicated panretinal degeneration in all of the patients.

The course of the decrease in the BCVA of each patient is shown in Figure 2. Due to the early involvement of the macula, the BCVA had decreased to worse than 0.1 (decimal), which is 1.0 logMAR units, in at least one eye by the thirties. The BCVA tended to decrease gradually after

initial visit. Then the BCVA deteriorated to worse than 0.1 (decimal) within a relatively short time in patients NA0039, NA0201, NA1209, and NA1201 (Fig. 2).

Fundus images.

Fundus photographs were obtained from all 9 patients (Fig. 3), and ultra-widefield FAF images were obtained from 8 patients (Fig. 4). All patients except NA0209 had severe degeneration accompanied by bone-spicule pigmentation around the arcade vessels and macular degeneration. FAF showed patchy and coalescent hypo-autofluorescent areas at the posterior pole which indicated atrophy of the retinal pigment epithelium (RPE). Fine hypo-autofluorescent patchy areas were present in the peripheral retina in all cases except NA0209. The fundus and FAF of case NA0209 appeared to be a much milder phenotype compared to those of the other patients; fundus showed minimum macular abnormalities, FAF showed hyperreflectivity in macular area, and small patchy hypo-autofluorescense at the fovea (Figure 5).

OCT images of all the cases are shown in Figure 6. The OCT images showed abnormalities in the outer retina, e.g., disrupted ellipsoid zone (EZ) and thinning of the outer nuclear layer. The EZ was totally absent in all cases, except case NA0209, and several fine hyperreflective structures, like tubulations, were found on the RPE in most of the eyes as shown by yellow arrows in Figure 6.

Progression of retinal degeneration in case NA0209.

The clinical manifestations of case NA0209 were much milder than those of the other patients; the patient had no bone-spicule pigmentation, fewer hypo-autofluorescent patchy areas, and relatively preserved BCVA. The changes of the FAF and OCT images of case NA0209 during a 5-year follow-up period are shown in Figure 5. FAF showed an increase in the number of fine hypo-autofluorescent patchy spots around the arcade vessels and the fovea. Similar features were found in the eyes of his sister (case NA1209 in Fig. 4). In addition, OCT showed a severe reduction of retinal thickness with the central retinal thickness reduced from 163 μm to 131 μm. These results indicated a progressive retinal degeneration both in the macular and peripheral retina. The AO fundus images at 21-years-of-age showed cone mosaics although they were sparsely distributed compared to those of normal control eyes (Fig. 5B). The cone densities at the 1° and 3° from the fovea on the nasal side were 11231/mm^2 and 7718/mm^2 respectively, and that at 3° on the temporal side was 8984/mm^2. As reference, the of cone densities in a normal control eye at 1° and 3° from the fovea on the nasal side and 3° on the temporal side were 31042/mm^2, 23283/mm^2, and 24333/mm^2, respectively.

Analyses of AO fundus images of surviving photoreceptor areas.

We obtained the AO fundus images of 8 patients except case NA1039. The images of one case (NA0048) were difficult to analyze because the quality was poor due to unsteady fixation. In general, AO fundus imaging has been used to detect and count the number of photoreceptors in eyes with hereditary retinal disorders. However, cone mosaics were detected in the AO images only in the eyes of case NA0209 (Fig. 5). Therefore, we focused on other retinal structures in the AO images.

The changes of AO images of the right eye of case NA0201 during a 4-year follow-up period are shown in Figure 7. Isolated, small, and deeply-colored areas were detected in the fundus photographs corresponding to the areas of the hyper-autofluorescence in the FAF images of the central macula. The remaining hyperreflective structures on the RPE in OCT images corresponded to the hyper-autofluorescent areas in the FAF images. The AO fundus images precisely identified the areas of hyper-autofluorescence in the FAF images, which presumably represented island-like residual photoreceptor areas and named “photoreceptor islands”. In contrast to their surrounding surfaces, the areas were homogenous even though the cone mosaics were invisible. The edges of the islands were partially covered by hyporeflective clumps (HRCs). HRCs were observed not only at the border of the islands but also around the photoreceptor islands. Higher magnified images showed that the small HRCs participated in the formation of the larger HRCs (Fig. 7 top right). The size of photoreceptor island appeared smaller and less homogenous after 4 years which made their borders unclear. The mean area of the residual photoreceptor island measured in AO fundus images

195 was reduced from 6.0 x 10^5 μm^2 in 2013 to 4.3 x 10^5 μm^2 in 2015, and to 2.9 x 10^5 μm^2 in 2017.
196 The BCVA decreased from 0.13 (decimal) in 2013 to 0.06 in 2015, and 0.02 in 2017. The
197 corresponding areas of the OCT images showed a decrease in retinal thickness due to a reduction of
198 the thickness of the outer nuclear layer (ONL, Fig. 7).
199 Similar AO findings were found in other 7 eyes; the right eye (Rt) and left eye (Lt) of NA1048,
200 NA0201Lt, NA1201Lt, NA0039Lt, NA0070Rt, and NA1209Lt. However, the quality of the AO
201 images of NA201Lt (BCVA; 0.1) and 1209Lt (BCVA; 0.02) were poor, and the borders of the
202 photoreceptor islands were too indistinct to analyze. In 5 eyes (NA0039Rt, NA1201Rt, NA0070Lt,
203 NA1209Rt, and NA1209Rt eyes) the photoreceptor islands could not be detected in the FAF or in
204 the AO images presumably due to a complete loss of the residual photoreceptor areas. The BCVA in
205 these eyes was close to total blindness and ranged from LP to 0.05 (decimal). In addition to the AO
206 image of NA0201Rt, those of NA1201Lt, NA0039Lt, and NA0070Rt eyes were followed for about
207 four years, and the baseline images are shown in Figure 8. The OCT images showed that the fine
208 structures appeared like outer retinal tubulations on the RPE in the corresponding areas. The course
209 of the reduction in the size of the photoreceptor islands measured in AO fundus images and BCVA
210 in NA0039Lt, NA0201Rt, NA1201Lt, and NA0070Rt are shown in Figure 8B. During the 4 year of
211 follow-up period, the size of the photoreceptor island in case NA1201Lt was reduced from 8.2 x
212 10^5 μm^2 to 4.8 x 10^5 μm^2, however the BCVA was maintained at 0.5 (decimal). On the other hand,

213 the size of photoreceptor islands in the other 3 eyes (NA0039Lt, NA0201Rt, and NA0070Rt)

214 decreased to less than 3.0 x 10^5 μm^2 with a reduction of the BCVA to <0.1(decimal). The AO

215 images of NA1048Rt and Lt were obtained only once and the sizes were 12.1 x 10^5 μm^2 and 25.1 x

216 10^5 μm^2 respectively (images not shown) with relatively preserved BCVA (0.5 in both eyes).

217

218 **Discussions**

219 Several *RP1* variants have been reported to cause adRP or arRP in Japanese patients [6, 7, 17-19].

220 The m1 variant had not been identified as a causative variant of arRP in a large Japanese RP cohort

221 study using targeted resequencing [18,19], although the m1 variant was present in 4.5% of RP

222 patients in our recent study [12]. The reason for this discrepancy might be that the m1 variant was

223 missed by targeted resequencing because the insertion of 328 nucleotides was too large to be

224 detected. Indeed, the m1 variant was first detected by Whole-Genome Sequence screening [12], and

225 our earlier targeted resequencing could not detect the m1 variant in case NA0201 although the m2

226 variant was detected [19]. This indicated that the m1 variant might be the cause of patients whose

227 causative genes had not been identified by targeted resequencing, especially in early onset and

228 severe RP cases with macular involvement.

229 Patients with the m1/m1 and m1/m2 variants appeared to have no significant differences in the

230 course of retinal degeneration; both genotypes shared phenotypic characteristics including severe

231 retinal degeneration with early macular involvement. In addition, clinical courses of our patients
232 resemble that of ARRP caused by other frameshift variants in *RP1*.Thus we speculate the disease
233 mechanism of m1 and m2 is the complete loss of function due to nonsense-mediated mRNA decay.
234 The early BCVA loss was caused by macular degeneration at a younger age which can be explained
235 by the expression of the protein encoded by *RP1* in the ciliary axoneme of both rods and cones [9,
236 10].
237 Our results indicated that all of our patients, except case NA0209, had an early onset of impaired
238 vision that occurred during the first decade of life. This was followed by a severe decrease of the
239 BCVA in the second and third decade which has been reported as a phenotype of arRP caused by
240 *RP1* variants [4, 6, 7, 11, 20]. Only case NA0209 had a relatively late onset retinal degeneration
241 compared to the other patients including his sibling. However, even in this patient, OCT showed a
242 progressive reduction of the retinal thickness and FAF showed a similar retinal degeneration pattern
243 as his sister. In addition, fundus AO images indicated that the cone density was reduced to one-third
244 of that of a normal control at 21-years-of-age. Therefore, his clinical findings might show the early
245 phase of severe retinal degeneration. The reason for the differences of the progression between the
246 two siblings was not determined but some other genetic factors rather than environmental factors
247 might be responsible for this because these siblings had been raised in a similar environment.

248 The FAF images are produced by retinoid byproducts of the visual cycle that accumulate in the
249 RPE [21], and they are assumed to be related to the remaining functional retina in eyes with
250 inherited retinal diseases [22, 23]. In the late stages of choroideremia, some patients have areas of
251 residual hyper-autofluorescence, called scalloped regions, surrounded by hypo-autofluorescent
252 areas [22, 23]. These hyper-autofluorescent areas are reported to be correlated with the areas of
253 surviving photoreceptors determined from multiple slices through the EZ in the OCT images [22,
254 23]. The size of these residual autofluorescent areas shrinks every year[24], and they have been
255 used to monitor the effectiveness of gene therapy in these types of patients [25]. Similar
256 autofluorescent areas were found in some eyes in our cohort. The high resolution AO fundus
257 images have allowed researchers to detect the subtle changes of the macular structures during the
258 course of retinal degeneration. Therefore, for the evaluation of the photoreceptor structure in
259 "scalloped regions" of choroideremia, our AO image analysis might be useful.
260 Our results showed that the course of reduction of the BCVA was composed of three phases. Most
261 patients had a reduction in the BCVA soon after the initial visit due to an involvement of the
262 macular area. This might be caused by the reduction of cone mosaics as observed in the AO images
263 of case NA209. However, the BCVA was relatively well preserved until the mid-20s, and then the
264 BCVA decreased in a relatively quickly (Fig. 2). The AO image analyses suggested that the
265 preserved photoreceptor islands were responsible for the maintained BCVA of >0.1(decimal). The

disruption of the photoreceptor islands appeared to lead to a further decrease in BCVA to nearly complete blindness. Indeed, the FAF and AO images did not detect any photoreceptor islands in near blind eyes such as the NA0039Rt, NA1201Rt, and NA1209Rt and Lt.

The relationships between the AO images and pathological changes of the retina have not been accurately determined mainly because of the limited number of studies of the high-resolution AO images. HRCs were found at the edge of photoreceptor islands but their origins are uncertain. Because melanin is the ocular pigment with the highest absorption in flood illumination near infrared AO imaging, it is possible that the HRCs are composed of melanin molecules and/or their derivatives. Some of the round HRCs observed *in vivo* in the degenerating retina with geographic atrophy were shown to be of similar in size and shape to ectopic RPE cells reported by histology [26]. If this is true, the detached RPE cells might migrate to the edge of the photoreceptor islands because the appearance and size of the HRCs in our study (Fig. 7) are identical to those in the previous report [26]. It is known that following the death of all photoreceptors, the RPE cells detach from Bruch's membrane and migrate to perivascular sites in the inner retina producing the bone spicule pigments [27]. It is possible that a similar migration of RPE is related to the loss of photoreceptor islands.

Our retrospective study has several limitations. The AO fundus images were analyzed from only 7 eyes because of difficulties in recording high quality images from eyes with poor fixation. In

addition, statistical analyses could not be performed due to the low number of images and different times of obtaining the images. In addition, not only the size but also the quality of photoreceptor island images would affect the BCVA because the BCVA of NA1201Lt was maintained at 0.5 in spite of a decrease in the size of photoreceptor islands. Future investigations of the size and quality of the photoreceptor islands using microperimetry might provide additional information that will help in making a prognosis of RP patients.

Another limitation is"photoreceptor island" is not a common feature of the RP. Usually in the advanced stage of RP, AO images can detect only mottled structures with unknown origin and "photoreceptor island" were found in a small portion of the eyes with RP. Thus our AO image analysis can be applied for the limited number of RP patients.

In conclusion, we have analyzed the phenotypic characteristics of arRP eyes carrying the m1 variant. These patients had severe retinal degeneration with early macular involvement as reported in arRP eyes caused by other *RP1* variants [4, 6, 7, 11, 20]. In the course of macular degeneration in our cohort, the AO images showed not only the reduction of the cone intensity in one patient but also showed the process of the reduction of the residual photoreceptor areas at the end stage of RP. These changes indicated that total blindness appeared to be related to the loss of the photoreceptor islands. Monitoring the fine retinal structures and the cone mosaics by AO fundus imaging could

provide further prognostic implications and can be used for the evaluation of new therapeutic applications.

Acknowledgements

The authors thank Professor Emeritus Duco Hamasaki of the Bascom Palmer Eye Institute for the discussions and editing the final version of the manuscript. This work was supported in part by the Japan Society for the Promotion of Science (JSPS) KAKENHI Grant Numbers 19K09928 to S.U and Takayanagi Retina Research Award to S.U.

References

1. Pierce EA, Quinn T, Meehan T, McGee TL, Berson EL, Dryja TP. Mutations in a gene encoding a new oxygen-regulated photoreceptor protein cause dominant retinitis pigmentosa. *Nat Genet* 1999;22:248-54.

2. Sullivan LS, Heckenlively JR, Bowne SJ, Zuo J, Hide WA, Gal A et al. Mutations in a novel retina-specific gene cause autosomal dominant retinitis pigmentosa. *Nat Genet* 1999;22:255-9.

3. Khaliq S, Abid A, Ismail M, Hameed A, Mohyuddin A, Lall P et al. Novel association of RP1 gene mutations with autosomal recessive retinitis pigmentosa. *J Med Genet* 2005;42:436-8.

4. Riazuddin SA, Zulfiqar F, Zhang QJ, Sergeev YV, Qazi ZA, Husnain T, Caruso R et al. Autosomal recessive retinitis pigmentosa is associated with mutations in RP1 in three consanguineous Pakistani families. *Invest Ophthalmol Vis Sci* 2005;46:2264-70.

5. Avila-Fernandez A, Corton M, Nishiguchi KM, Munoz-Sanz N, Benavides-Mori B, Blanco-Kelly F et al. Identification of an RP1 prevalent founder mutation and related phenotype in Spanish patients with early-onset autosomal recessive retinitis. *Ophthalmology* 2012;119:2616-21.

6. Kurata K, Hosono K, Hotta Y. Clinical and genetic findings of a Japanese patient with RP1-related autosomal recessive retinitis pigmentosa. *Doc Ophthalmol* 2018;137:47-56.

7. Verbakel SK, van Huet RAC, den Hollander AI, Geerlings MJ, Kersten E, Klevering BJ et al. Macular dystrophy and cone-rod dystrophy caused by mutations in the RP1 gene: Extending the RP1 disease spectrum. *Invest Ophthalmol Vis Sci* 2019;60:1192-203.

8. Riera M, Abad-Morales V, Navarro R, Ruiz-Nogales S, Mendez-Vendrell P, Corcostegui B et al. Expanding the retinal phenotype of RP1: from retinitis pigmentosa to a novel and singular macular dystrophy. *Br J Ophthalmol* 2019. doi:10.1136/bjophthalmol-2018-313672

9. Liu Q, Zhou J, Daiger SP, Farber DB, Heckenlively JR, Smith JE et al. Identification and subcellular localization of the RP1 protein in human and mouse photoreceptors. *Invest Ophthalmol Vis Sci* 2002;43:22-32.

10. Liu Q, Lyubarsky A, Skalet JH, Pugh EN, Pierce EA et al. RP1 is required for the correct stacking of outer segment discs. *Invest Ophthalmol Vis Sci* 2003;44:4171-83.

11. El Shamieh S, Boulanger-Scemama E, Lancelot M-E, Antonio A, Demontant V, Condroyer C et al. Targeted next generation sequencing identifies novel mutations in RP1 as a relatively common cause of autosomal recessive rod-cone dystrophy. *BioMed Res Int* 2015. doi:10.1155/2015/485624

12. Nikopoulos K, Cisarova K, Quinodoz M, Koskiniemi-Kuendig H, Miyake N, Farinelli P et al. A frequent variant in the Japanese population determines quasi-Mendelian inheritance of rare retinal ciliopathy. *Nat Commun* 2019;10:2884. doi: 10.1038/s41467-019-10746-4.

13. Nakanishi A, Ueno S, Kawano K, Ito Y, Kominami T, Yasuda S et al. Pathologic changes of cone photoreceptors in eyes with occult macular dystrophy. *Invest Ophthalmol Vis Sci* 2015;56:7243-9.

14. Ueno S, Kawano K, Ito Y, Ra E, Nakanishi A, Nagaya M et al. Near-infrared reflectance imaging in eyes with acute zonal occult outer retinopathy. *Retina* 2015;35:1521-30.

15. Ueno S, Nakanishi A, Kominami T, Ito Y, Hayashi T, Yoshitake K et al. In vivo imaging of a cone mosaic in a patient with achromatopsia associated with a GNAT2 variant. *Jpn J Ophtalmol* 2017;61:92-8.

16. Ueno S, Nakanishi A, Sayo A, Kominami T, Ito Y, Hayashi T et al. Differences in ocular findings in two siblings: one with complete and other with incomplete achromatopsia. *Doc Ophthalmol* 2017;134:141-47.

17. Kawamura M, Wada Y, Noda Y, Itabashi T, Ogawa SI, Sato H et al. Novel 2336-2337 delCT mutation in RP1 gene in a Japanese family with autosomal dominant retinitis pigmentosa. *Am J Ophthalmol* 2004;137:1137-39.

18. Oishi M, Oishi A, Gotoh N, Ogino K, Higasa K, Iida K et al. Comprehensive molecular diagnosis of a large cohort of Japanese retinitis pigmentosa and Usher syndrome patients by next-generation sequencing. *Invest Ophthalmol Vis Sci* 2014;55:7369-75.

19. Koyanagi Y, Akiyama M, Nishiguchi KM, Momozawa Y, Kamatani Y, Takata S et al. Genetic characteristics of retinitis pigmentosa in 1204 Japanese patients. *J Med Genet* 2019; 56: 662-70.

20. Chen LJ, Lai TYY, Tam POS, Chiang SWY, Zhang X, Lam S et al. Compound heterozygosity of two novel truncation mutations in RP1 causing autosomal recessive retinitis pigmentosa. *Invest Ophthalmol Vis Sci*. 2010;51:2236-42.

21. Schmitz-Valckenberg S, Holz FG, Bird AC, Spaide RF. Fundus autofluorescence imaging: review and perspectives. *Retina* 2008;28:385-409.

22. Aleman TS, Han G, Serrano LW, Fuerst NM, Charlson ES, Pearson DJ et al. Natural history of the central structural abnormalities in choroideremia: A prospective cross-sectional study. *Ophthalmology* 2017;124:359-73.

23. MacLaren RE, Groppe M, Barnard AR, Cottriall CL, Tolmachova T, Seymour L et al. Retinal gene therapy in patients with choroideremia: initial findings from a phase 1/2 clinical trial. *Lancet* 2014;383:1129-37.

24. Jolly JK, Edwards TL, Moules J, Groppe M, Downes SM, MacLaren RE. A qualitative and quantitative assessment of fundus autofluorescence patterns in patients with choroideremia. *Invest Ophthalmol Vis Sci* 2016;57:4498-503.

379 25. Xue K, Jolly JK, Barnard AR, Rudenko A, Salvetti AP, Patricio MI et al. Beneficial effects
380 on vision in patients undergoing retinal gene therapy for choroideremia. *Nat Med* 2018;24:1507-12.
381 26. Gocho K, Sarda V, Falah S, Sahel JA, Sennlaub F, Benchaboune M et al. Adaptive optics
382 imaging of geographic atrophy. *Invest Ophthalmol Vis Sci* 2013;54:3673-80.
383 27. Milam AH, Li ZY, Fariss RN. Histopathology of the human retina in retinitis pigmentosa.
384 *Prog Retin Eye Res* 1998;17:175-205.
385

Table. Demographic data of 9 Japanese ARRP patients with 4052_4053ins328/p.Tyr1352Alafs*9 in *RP1*

Family No	Patient No	Sex	Age at onset	Age at initial visit	BCVA (Decimal) at initial visit		Visual field at initial visit	Electroretinogram	Age at finial visit	BCVA (Decimal) at final visit		Pathogenic alleles		AO finidngs	
					RE	LE				RE	LE	Allele 1	Allele 2	RE	LE
1	NA0039	F	6	21	0.8	0.8	Central island	ND	34	LP	0.01	m1	m1	No photorecepotor island	Photoreceptor island
1	NA1039	M	6	27	0.6	0.6	Central island	NA	33	0.6	0.4	m1	m1	NA	NA
2	NA0048	F	5	12	0.6	0.7	Paracentral scotoma, peripheral constriction	ND	19	0.04	0.2	m1	m1	Low quality	Low quality
2	NA1048	M	5	14	0.9	0.9	Paracentral scotoma, peripheral constriction	ND	22	0.5	0.5	m1	m1	Photoreceptor island	Photoreceptor island
3	NA0070	F	6	25	0.4	0.5	Paracentral scotoma, peripheral constriction	Severely reduced	39	0.05	0.2	m1	m1	Photoreceptor island	No photorecepotor island
4	NA0201	M	6	15	0.6	0.5	Central island	ND	32	HM	0.1	m1	m2	Photoreceptor island	Photoreceptor island
4	NA1201	F	6	8	0.8	0.8	Paracentral scotoma, peripheral constriction	ND	36	HM	0.5	m1	m2	No photorecepotor island	Photoreceptor island
5	NA0209	M	15	20	1	1	Paracentral scotoma	Reduced	26	0.8	0.6	m1	m2	Cone mosaic	Cone mosaic
5	NA1209	F	6	19	0.4	0.7	Paracentral scotoma, peripheral constriction	ND	30	HM	0.02	m1	m2	No photorecepotor island	Photoreceptor island

ARRP=autosomal recessive retinitis pigmentosa BCVA= best corrected visual acuity; F=female; HM=hand motion; LE=left eye; LP=light perception; M=male; NA=not available; ND=not detectable; No.=number; RE=right eye; m1=c.4052_4053ins328/p.Tyr1352Alafs*9 (Alu insertion); m2=c.4196delG/p.Cys1399Leufs*5

Figure Legends

Figure 1. Pedigree charts of 9 autosomal recessive retinitis pigmentosa cases carrying the m1 variant (c.4052_4053ins328/p.Tyr1352Alafs*9) in the *RP1* gene.

The m2 variant (c.4196delG/p.Cys1399Leufs*5) was found in 2 families. There was no reported consanguinity in any of these pedigrees. Probands are shown by the arrows.

Figure 2. Graph showing the course of the best-corrected visual acuity over time in all eyes from our cohort.

Snellen visual acuity was converted to the logarithm of the minimum angle of resolution (logMAR). R; right L; left

Figure 3. **Fundus color photographs of the right eye of the 9 patients from 5 families (1-5) with autosomal recessive retinitis pigmentosa caused by a variant of the *RP1* gene; c.4052_4053ins328/p.Tyr1352Alafs*9 (m1).**

The age of the patients at which the photograph was taken is shown. All the patients except NA0209 had severe panretinal degeneration including macula. Y.O. ; year old .

Figure 4. Fundus autofluorescence (FAF) images of the right eye of 8 patients from 5 families (1-5).

The age of the patients at which the photograph was taken is shown. All patients except NA0209 had patchy and coalescent hypo-autofluorescent areas including macula. Y.O. ; year old .

Figure 5. Multimodal images in case NA0209.

a. Changes of retinal images during the follow-up period. Fundus autofluorescence (FAF, upper) shows fine hypo-autofluorescent patchy spots around the arcade vessels and at the fovea appeared during 5 years. The OCT images show a marked reduction of the retinal thickness in 5 years. Arrows indicate the residual EZ at 20-years-of-age which disappeared in 5 years. The scale bar is 200 μm.

b. Adaptive optics (AO) fundus images of case NA0209 at 21-years-of-age. A montage image is shown on the left. Magnified images of the white square (at 3 degrees from the central fovea on the temporal side and 1 and 3 degrees on the nasal side; shown as T3, N1and N3 respectively) in the montage image are shown. For comparison the AO images of a normal control at 3 degrees from the central fovea on the temporal side is shown (N3 Normal). The scale bar is 20 μm in the magnified AO images as well.

Figure 6. Optical coherence tomographic (OCT) images of the right eye of the 9 patients from 5 families (1-5). The OCT images shows thinning of the retina and abnormalities in the outer retina in all cases. Several fine hyperreflective structures can be seen on the RPE shown by the yellow arrows.

Figure 7. Progressive reduction of surviving photoreceptor areas (photoreceptor islands) in the right eye of case NA0201.

Fundus photograph (top left) shows a deep colored area in the central macula which was detected as a hyper autofluorescence area in fundus autofluorescence (FAF, top middle) images. The white squares in the color fundus photograph and FAF area corresponds to fundus AO images below. Successive AO images were recorded on June 2013, January 2015, and January 2017. The OCT images obtained on the same days are shown on the right of each AO fundus image, and the scanned area is shown by the dotted arrows in the AO fundus images. Illustrative images of the photoreceptor islands are shown at the bottom left of each AO image. The size of photoreceptor islands decreases progressively. The magnified image of the white square in the AO fundus image on June 2013 is shown at the top right. The edge of the photoreceptor island is partially covered by hyporeflective clumps (HRCs). Small HRCs participate to form the large clumps. HRCs surrounding the

photoreceptor island are shown in arrows and HRCs seen around the photoreceptor island are shown in arrow heads.

Figure 8. Findings of NA1201 left, NA0039 left, and NA0070 right eyes

a. Multimodal images of photoreceptor islands. The color fundus photograph (top left) and fundus autofluorescence (FAF; top right), AO fundus image, and OCT image of each eye are shown. The area surrounded by the white line in the color fundus and FAF images correspond to the montage of the AO fundus images (middle). The first recorded AO fundus images of each patient (baseline of analysis) and OCT images (below) on the same day are shown. The scanned areas for the OCT images are shown by the yellow dotted arrows in the AO fundus images. The fundus and FAF images obtained on the closest day to the AO images are shown. Illustrations of the photoreceptor islands are shown at the upper left of each AO fundus image. Hyper autofluorescence areas in the central macula detected in FAF are clearly visible in the AO fundus images.

b. Reduction in the size of the photoreceptor islands in four eyes (three eyes from A and 1 eye from Figure 4). The size of the photoreceptor island gradually decrease. The visual acuity (decimal) at each time point is also shown.

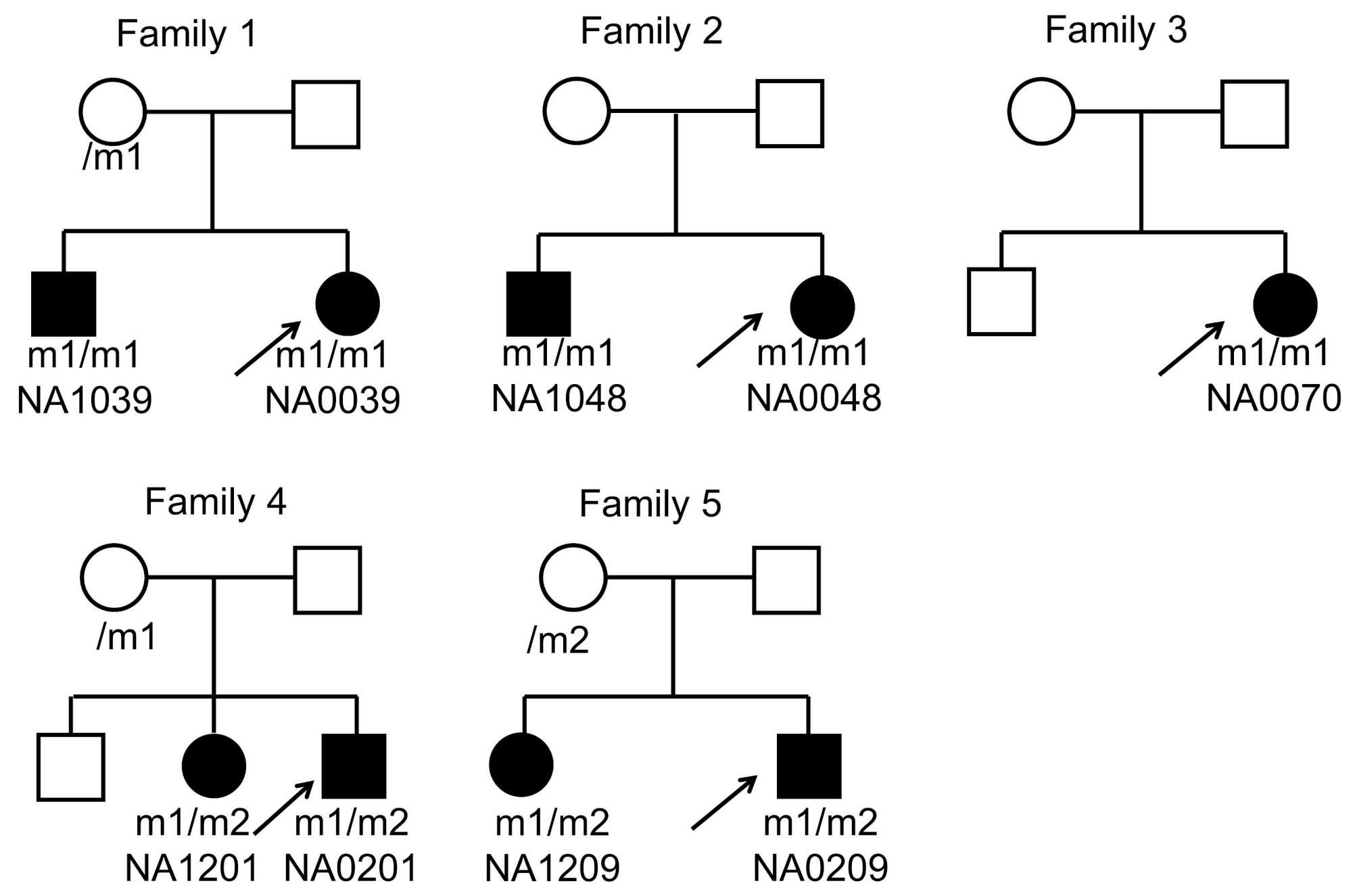
Family 1
/m1
m1/m1
NA1039
m1/m1
NA0039
Family 2
m1/m1
NA1048
m1/m1
NA0048
Family 3
m1/m1
NA0070
Family 4
/m1
m1/m2
NA1201
m1/m2
NA0201
Family 5
/m2
m1/m2
NA1209
m1/m2
NA0209

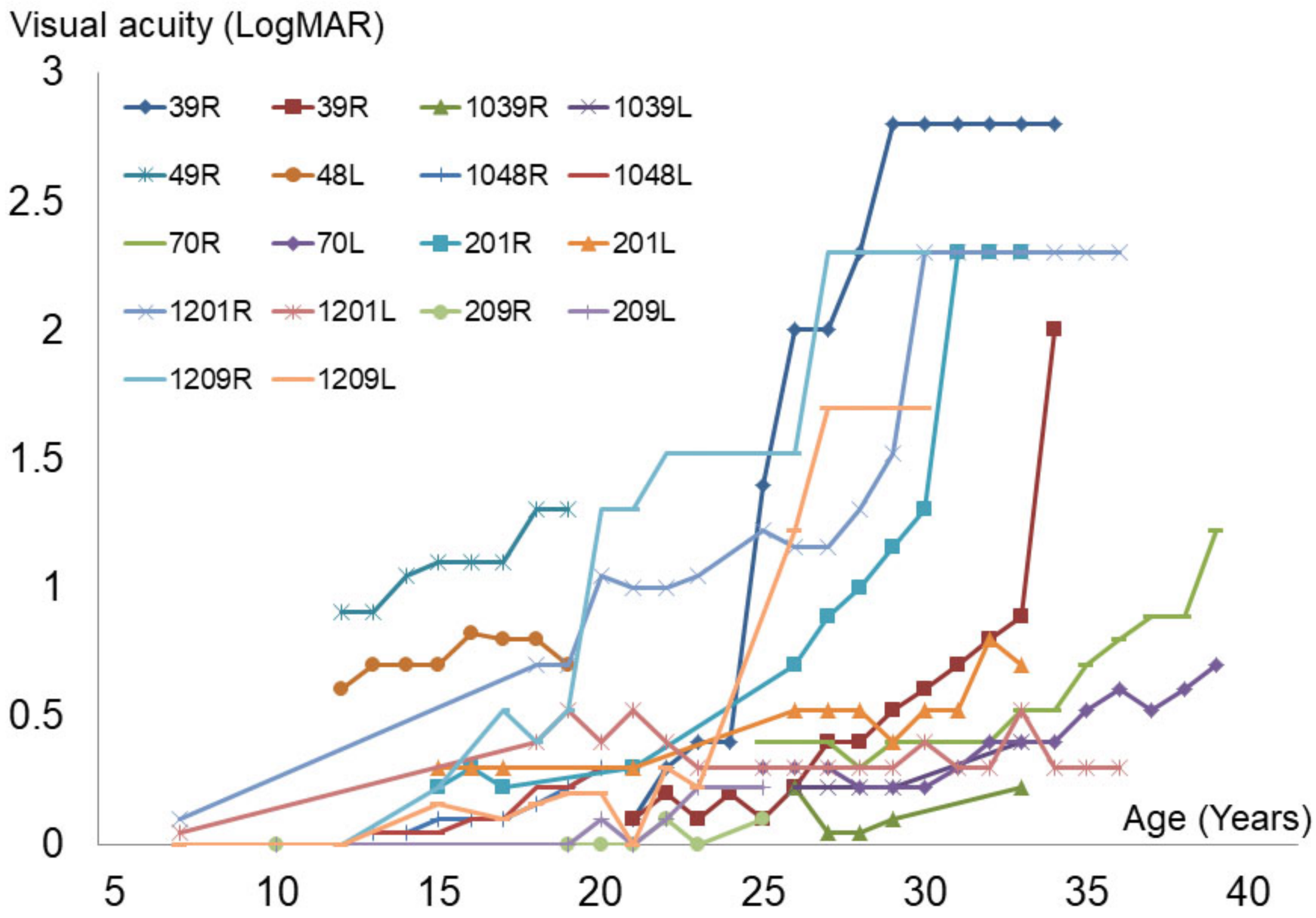

Graph showing the course of the best-corrected visual acuity over time in all eyes from our cohort. Snellen visual acuity was converted to the logarithm of the minimum angle of resolution (LogMAR). R; right L; left

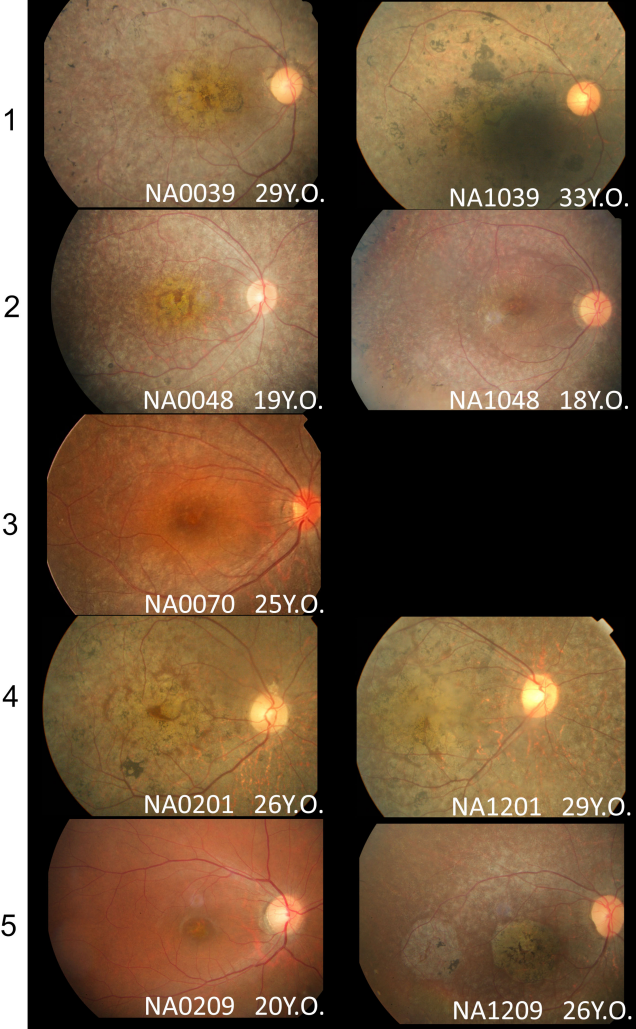
1
NA0039 29Y.O.
NA1039 33Y.O.
2
NA0048 19Y.O.
NA1048 18Y.O.
3
NA0070 25Y.O.
4
NA0201 26Y.O.
NA1201 29Y.O.
5
NA0209 20Y.O.
NA1209 26Y.O.

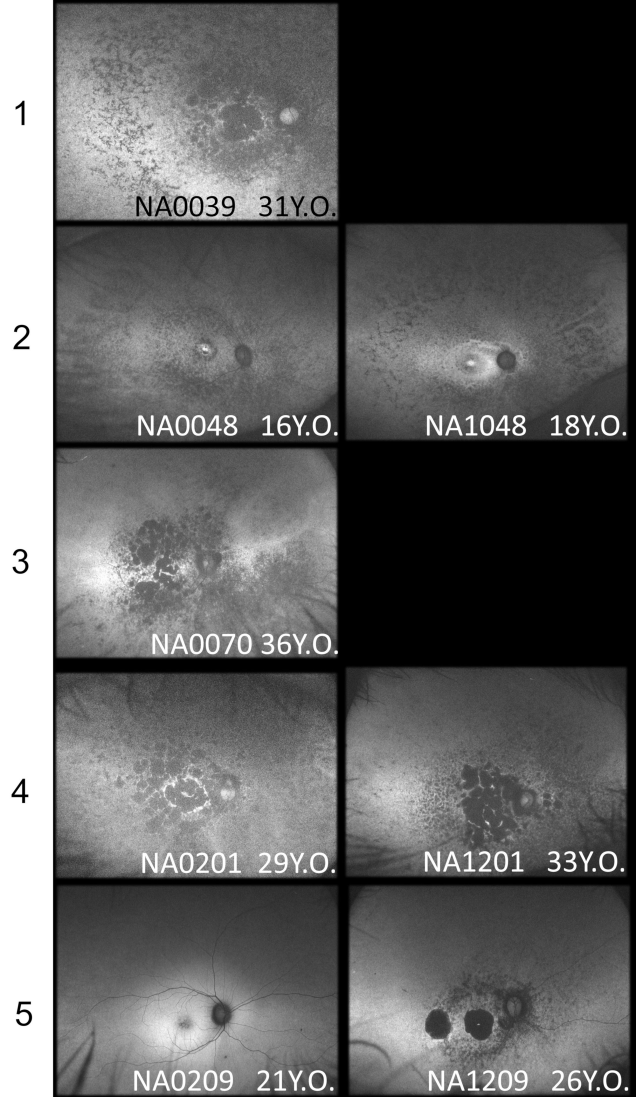
1
NA0039 31Y.O.
2
NA0048 16Y.O.
NA1048 18Y.O.
3
NA0070 36Y.O.
4
NA0201 29Y.O.
NA1201 33Y.O.
5
NA0209 21Y.O.
NA1209 26Y.O.

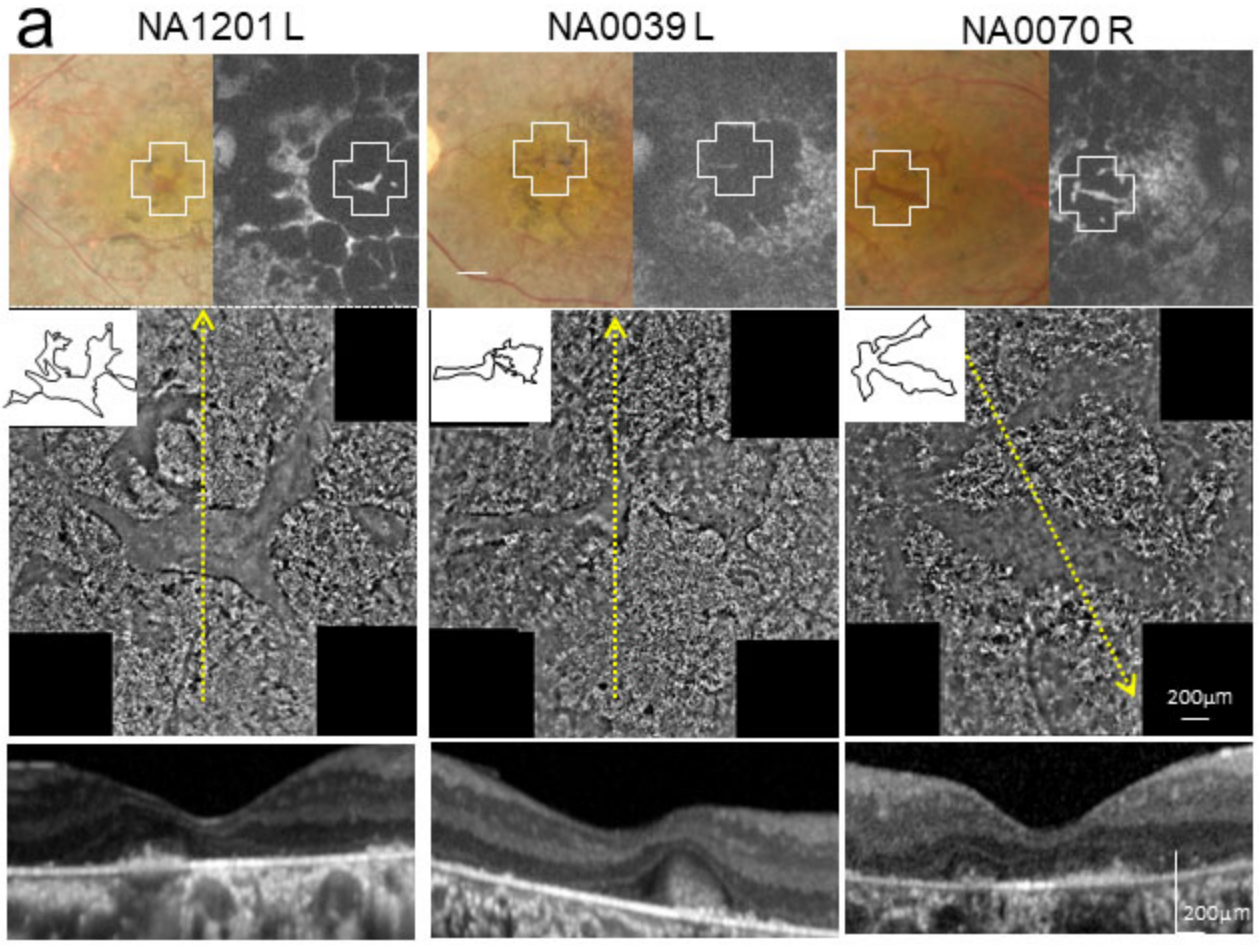
a
NA1201 L
NA0039 L
NA0070 R
200μm
200μm

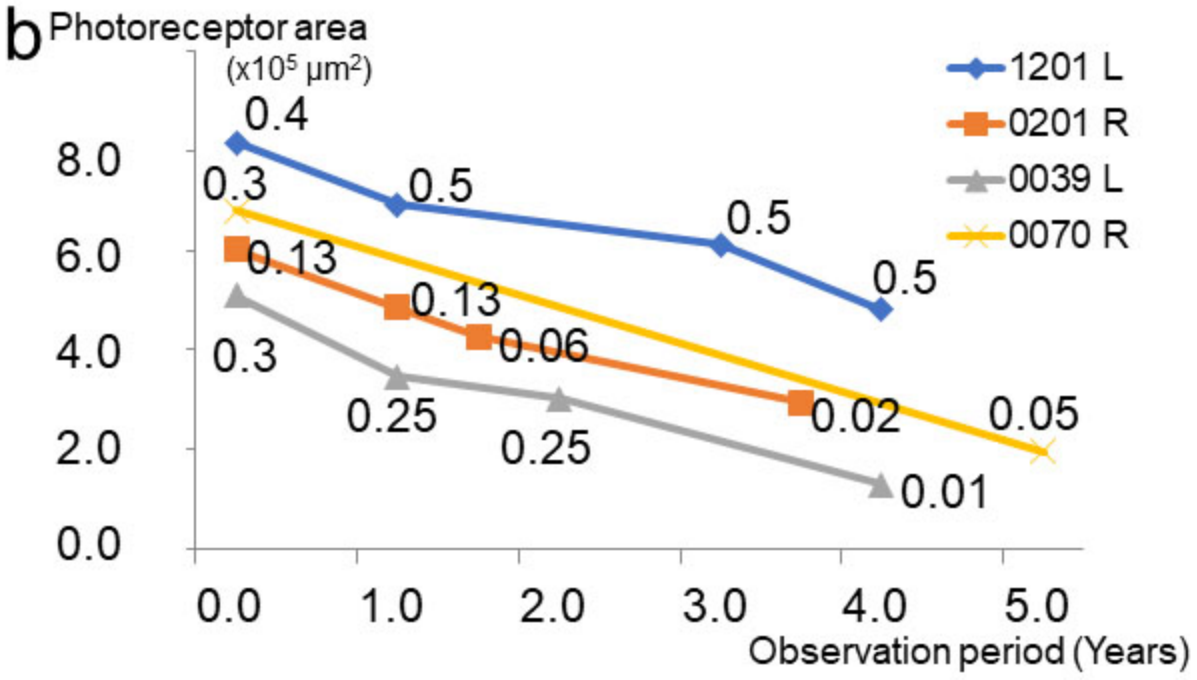
b
Photoreceptor area
(x10⁵ μm²)
8.0
6.0
4.0
2.0
0.0
0.0
1.0
2.0
3.0
4.0
5.0
Observation period (Years)
1201 L
0201 R
0039 L
0070 R
0.4
0.3
0.5
0.5
0.5
0.13
0.13
0.06
0.02
0.3
0.25
0.25
0.01
0.05

1

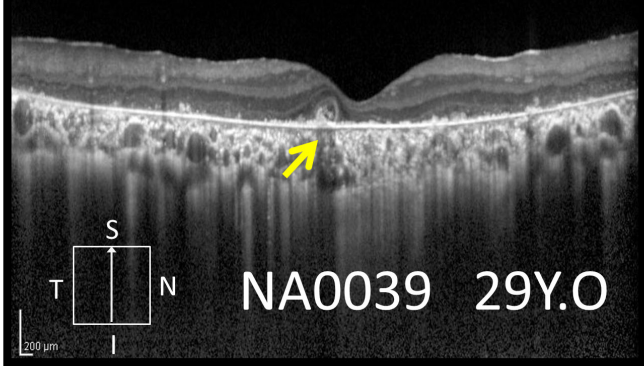
S
T
N
I
200 µm
NA0039 29Y.O

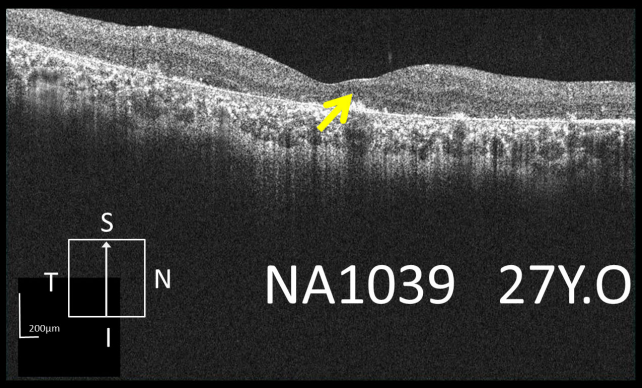
S
T
N
I
200µm
NA1039 27Y.O

2

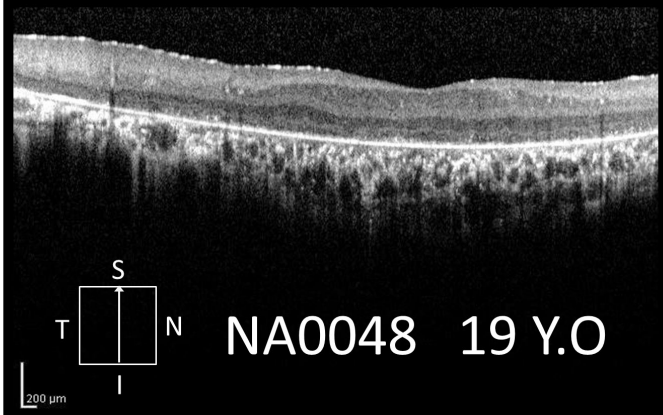
S
T
N
I
200 µm
NA0048 19 Y.O

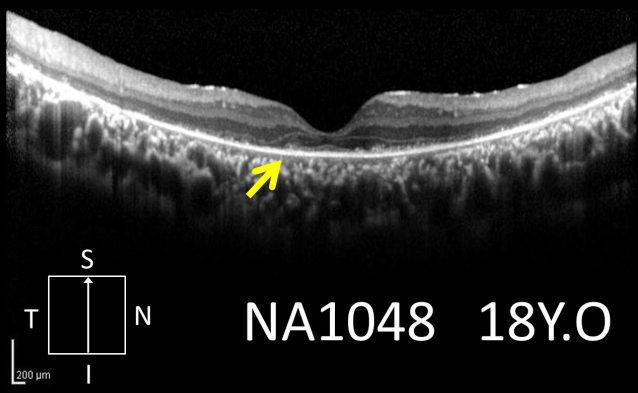
S
T
N
I
200 µm
NA1048 18Y.O

3

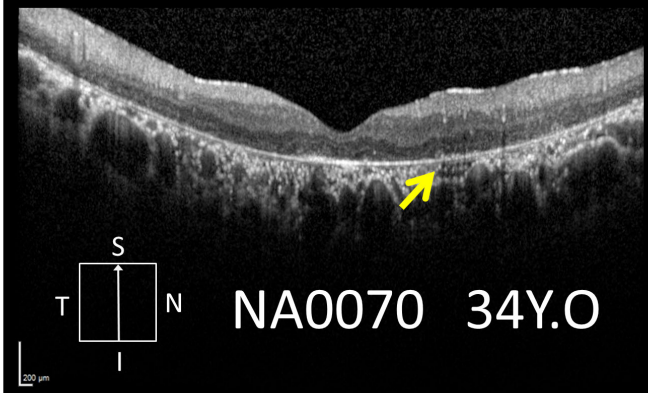
S
T
N
I
200 µm
NA0070 34Y.O

4

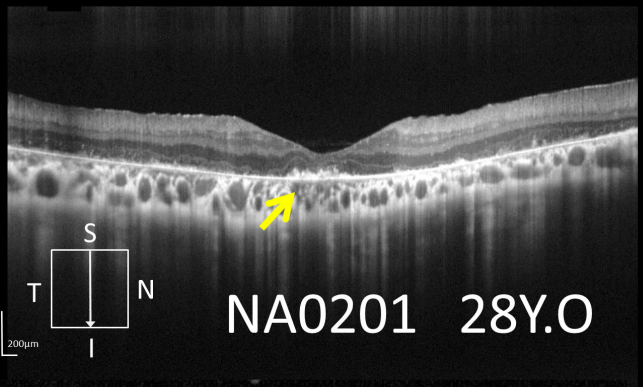
S
T
N
I
200µm
NA0201 28Y.O

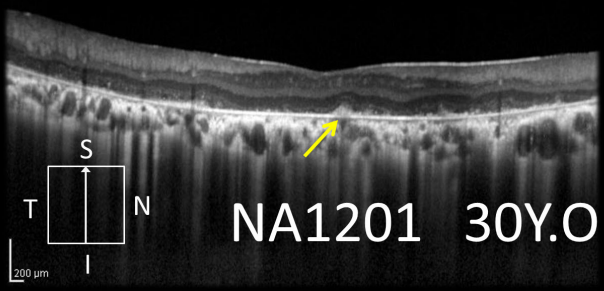
S
T
N
I
200 µm
NA1201 30Y.O

5

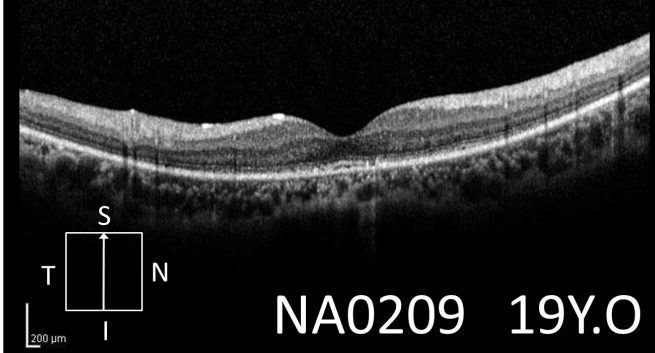
S
T
N
I
200 µm
NA0209 19Y.O

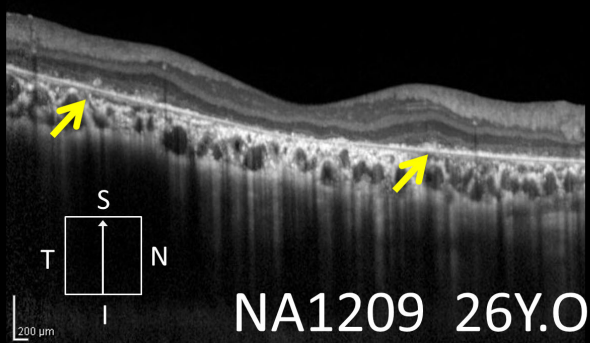
S
T
N
I
200 µm
NA1209 26Y.O

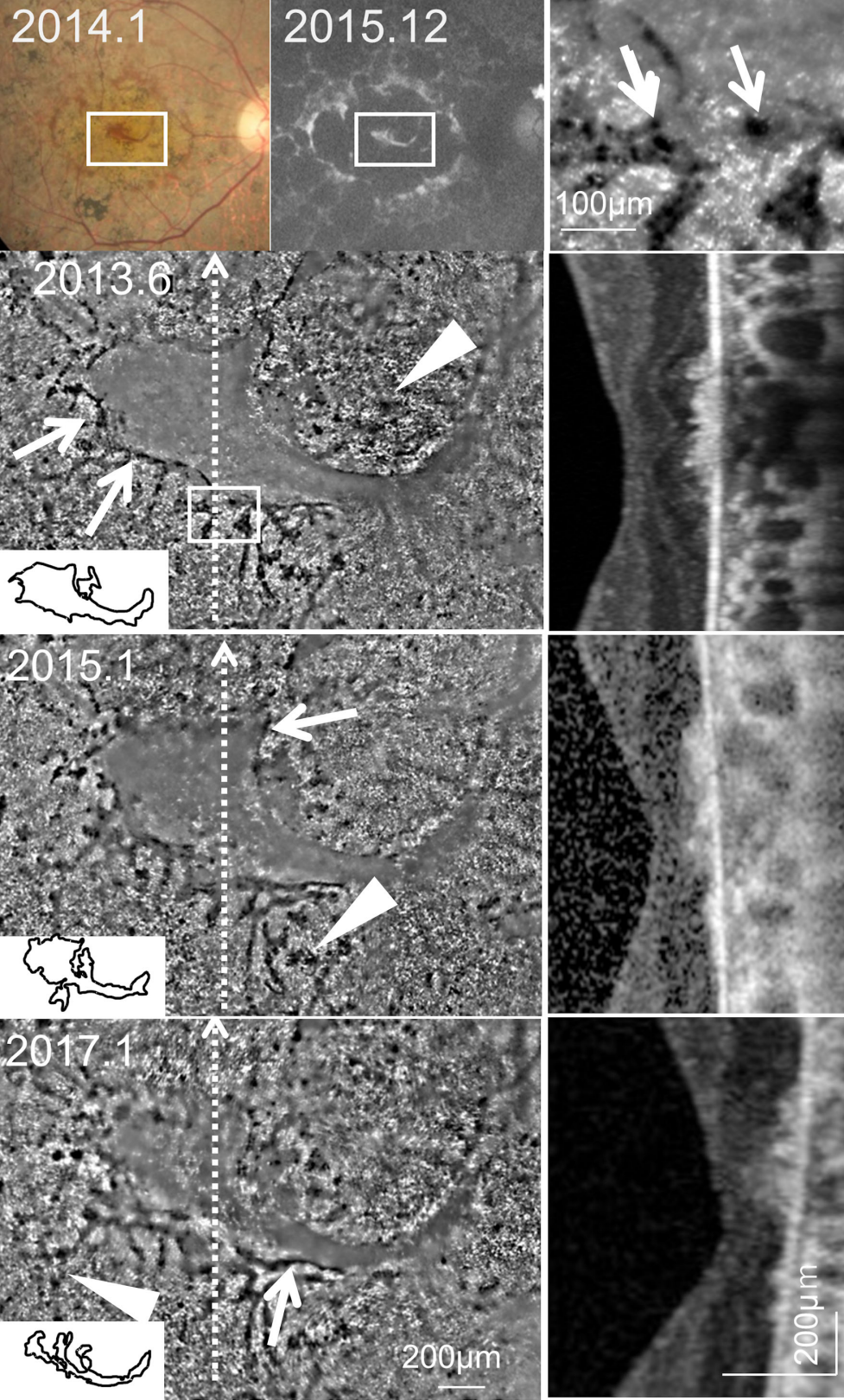
2014.1
2015.12
100μm
2013.6
2015.1
2017.1
200μm
200μm

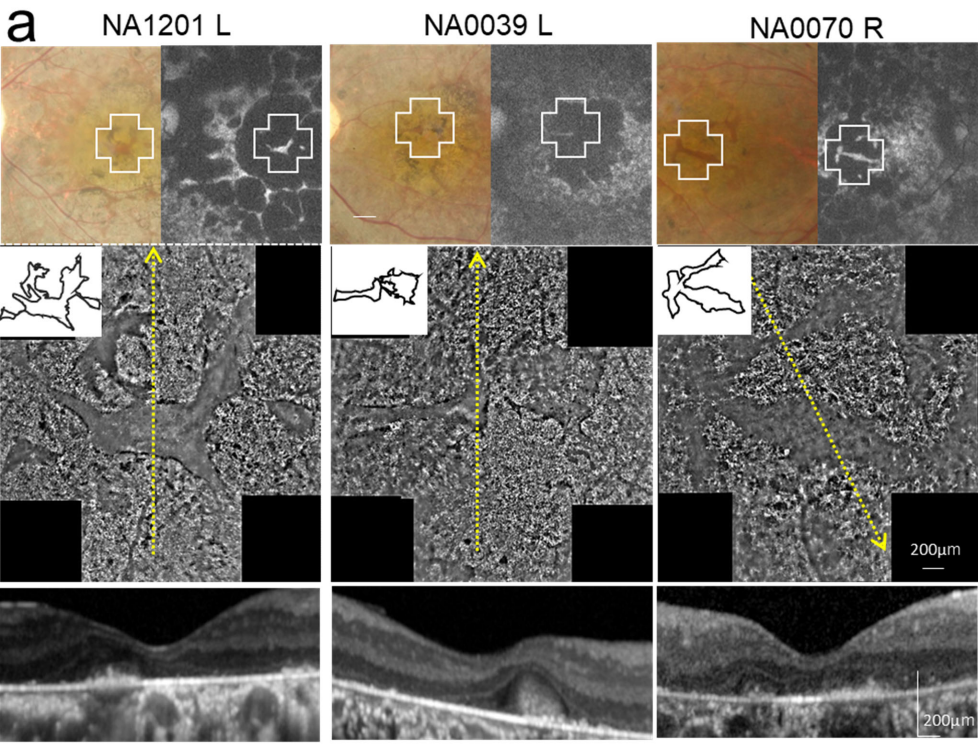
a
NA1201 L
NA0039 L
NA0070 R
200μm
200μm

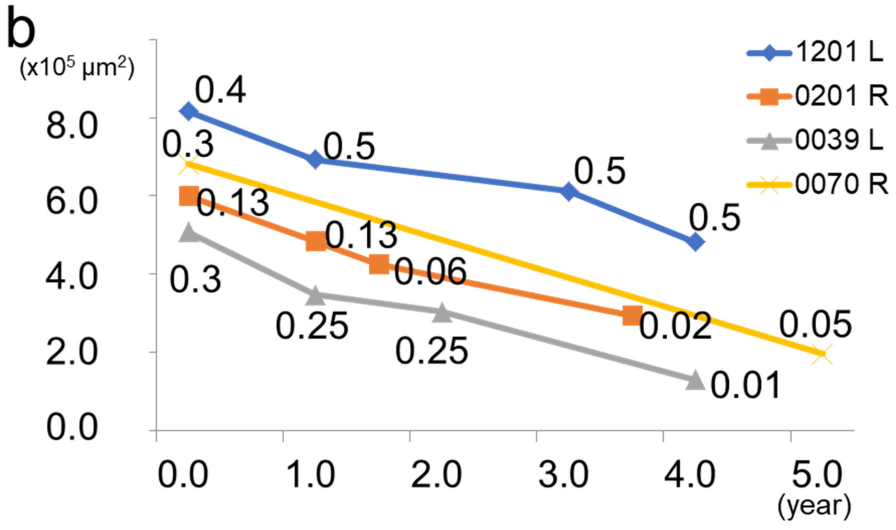
b
(x10^5 μm^2)
8.0
6.0
4.0
2.0
0.0
0.0
1.0
2.0
3.0
4.0
5.0
(year)
1201 L
0201 R
0039 L
0070 R
0.4
0.3
0.5
0.5
0.5
0.13
0.13
0.06
0.02
0.05
0.3
0.25
0.25
0.01